Journal of Engineering for Gas Turbines and Power. Received July 11, 2019;
Accepted manuscript posted 1 October, 2019. DOI:10.1115/1.4045077

Volume 142, Issue 4, April 2020, Article number 041016
Paper: number GTP-1447

Modelling Geared Turbofan and Open Rotor Engine Performance for Year-2050 Long-range and Short-range Aircraft

Francesco S. Mastropierro[1]
Cranfield University
Centre for Propulsion Engineering, Cranfield University, College Road, Cranfield, MK43 0AL, United Kingdom
francesco.mastropierro@cranfield.ac.uk
ASME Student Member

Joshua Sebastiampillai
Cranfield University
Centre for Propulsion Engineering, Cranfield University, College Road, Cranfield, MK43 0AL, United Kingdom
j.sebastiampillai@cranfield.ac.uk

Florian Jacob
Cranfield University
Centre for Propulsion Engineering, Cranfield University, College Road, Cranfield, MK43 0AL, United Kingdom
florianjacob.berlin@web.de

Andrew Rolt
Cranfield University
Centre for Propulsion Engineering, Cranfield University, College Road, Cranfield, MK43 0AL, United Kingdom
a.rolt@cranfield.ac.uk

ABSTRACT

The paper provides design and performance data for two envisaged year-2050 engines: a geared high bypass turbofan for intercontinental missions and a contra-rotating pusher open rotor targeting short to medium range aircraft. It defines component performance and cycle parameters, general arrangements, sizes and weights. Reduced thrust requirements reflect expected improvements in engine and airframe

[1] Corresponding author.

technologies. Advanced simulation platforms have been developed to model the engines and details of individual components.

The engines are optimized and compared with 'baseline' year-2000 turbofans and an anticipated year-2025 open rotor to quantify the relative fuel-burn benefits. A preliminary scaling with year-2050 'reference' engines, highlights trade-offs between reduced specific fuel consumption (SFC) and increased engine weight and diameter. These parameters are converted into mission fuel burn variations using linear and non-linear trade factors.

The final turbofan has an optimized design-point bypass ratio of 16.8, and a maximum overall pressure ratio of 75.4, for a 31.5% TOC thrust reduction and a 46% mission fuel burn reduction per passenger kilometer compared to the respective 'baseline' engine-aircraft combination. The open rotor SFC is 9.5% less than the year-2025 open rotor and 39% less than the year-2000 turbofan, while the TOC thrust increases by 8% versus the 2025 open rotor, due to assumed increase in passenger capacity. Combined with airframe improvements, the final open rotor-powered aircraft has a 59% fuel-burn reduction per passenger kilometer relative to its baseline.

INTRODUCTION

Civil aviation plays a crucial role in the modern global economy. Air passenger traffic reached 7.7 trillion revenue passenger kilometers (RPK) in 2017 [1], with average growth rates of more than 4% per annum over the last decade expected to continue for two more decades at least [2, 3]. Consequently, harmful emissions (CO2, NOx) and noise are also increasing and generating environmental concerns that are pushing aviation stakeholders to design ever more efficient aircraft components and to research new technologies. Specific goals have been set by the Advisory Council for Aviation Research and Innovation in Europe (ACARE) in 'Flightpath 2050' [4]. A 75% cut in CO2 emission and 90% NOx reduction per RPK, stet 65% noise attenuation are targeted for new

aircraft and engines in 2050, compared to those in service in year 2000. These improvements are expected to come from advanced airframe aerodynamics and structures, where laminar flow [5], truss-braced high aspect ratio wings [6, 7] and blended wing body [8] architectures are proposed, and also from the engines, where turboelectric or hybrid-electric propulsion [9], hydrogen fuel [10] and more-complex thermodynamic cycles [11] are being studied.

The ULTIMATE project [12] has investigated open-rotor technology and other disruptive engine concepts including composite cycles and pressure-rise combustion to improve core thermal efficiency and reduce emissions. In order to provide proper assessments of these more-advanced technologies and the resulting novel engine layouts, it is first necessary to predict realistic and comprehensive performance parameters for more-conventional engines for the year 2050. This paper reviews technology assumptions and performance parameters for two engines that between them may represent the majority of the civil-aviation market. Optimisation studies are performed on these engine cycles to minimize their mission fuel burns when installed in their respective year-2050 aircraft.

PRESENTATIONS OF MODELS

A geared high-bypass ratio turbofan engine (TF2050) is envisaged for long-range intercontinental missions, while a geared contra-rotating open-rotor engine (GOR2050) targets shorter routes. The powerplants are mounted on advanced tube-and-wing aircraft (ATW), with reduced drag and thrust requirements relative to current

technology aircraft [13]. The software used for engine modelling and calculations is version 3.6.14 of the commercially-available 'Propulsion Object Oriented Simulation Software' (PROOSIS), developed by Empresarios Agrupados [14]. Weight estimations are run using WeiCo 9.6 from Chalmers University, while Simulia Isight 5.9-4 is utilized for running optimisation studies.

Representative year-2000-state-of-the-art 'baseline engines' are modelled based on previous works [15]. These allow direct comparison with the year-2050 'reference' engines, which feature the presumed technology improvements. The baseline engine for the long-range mission (LR2000) mirrors the specification of the Trent 772B-60 mounted on an Airbus A330-300. For the short-range mission the baseline turbofan is similar to a CFM56-5B fitted on an Airbus A320 [16]. Appendix A summarizes the main performance parameters for 'Top-of-Climb' (TOC) cases, chosen as the design points, and also for cruise and End-of-Runway (EOR) take-off cases.

MODELLING ASSUMPTIONS FOR YEAR-2050 REFERENCE ENGINES

The TF2050 is assumed to represent the mid-century evolutionary limit of existing engine architectures. It features a reduction gearbox between the high-speed low pressure turbine (LPT), which drives the intermediate pressure compressor (IPC) directly, and the low-speed fan, as shown in Fig. 1. The high pressure turbine (HPT) and the high-pressure compressor (HPC) both feature tip clearance control to reduce over-tip leakage losses and maintain high component efficiencies despite the high overall pressure ratio and reduced core size.

The TF2050 is designed at cruise, where the engine would spend the majority of its operating time, but cooled cooling air is utilized during take-off and climb conditions to permit higher gas-path temperatures without sacrificing component life. The component specifications act as direct inputs for performance calculations. Basic component efficiencies for both the TF2050 and the GOR2050 are broadly consistent with the NASA projections outlined in [9].

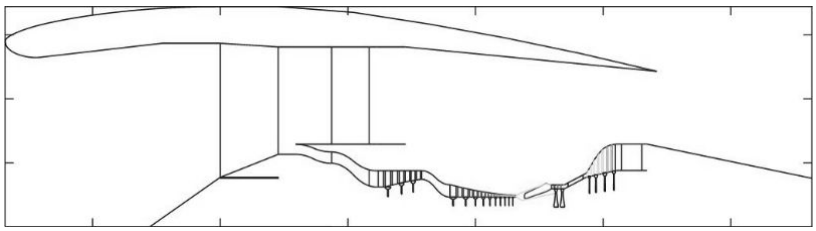

Figure 1: Schematic configuration of TF2050

Intake/Nozzles

A 0.3% pressure loss is introduced in the intake. Hot and cold nozzles are treated as separate exhausts; the thrust coefficients are constant over the flight envelope.

Fan

Design pressure ratio and efficiency are defined for core and bypass sections. The fan core section pressure rise is modelled as 72.7% that of the bypass section. The fan diameter is limited to 3.5 m for physical integration with the airframe.

IPC/HPC

Pressure ratios and design-point polytropic efficiencies are determined. The HPC delivery temperature is limited to 880 K at cruise for cooling and structural integrity

reasons. A penalty on isentropic efficiency is applied to the HPC, to account for the increasing importance of tip leakage effects over small blades, according to [17].

Combustor

The engine is expected to feature an efficient lean-burn direct injection combustor. A 3% pressure loss is assumed, with a combustion efficiency of 99.95%. Dissociation is not taken into account. The fuel heating value (LHV) is kept fixed at 42.8 MJ/kg for all cases.

HPT

By 2050 it seems reasonable to assume use of ceramic matrix composite (CMC) materials for nozzle guide vanes [18], which would only need internal convection cooling. However, the rotor blades still use nickel-based alloys with thermal barrier coatings. The calculations assume a fixed 6.3% compressor air offtake for HPT cooling throughout the flight envelope, and a hard limit of 1400 K for blade metal temperature is always respected. The HPT isentropic efficiency is penalized by half of the value for the HPC to account for tip leakage effects.

LPT

Uncooled titanium aluminide blading is anticipated.

Turbine isentropic efficiency

Defined at the cruise design point.

Off-design performance

Maps for turbomachinery components are respectively selected from [19-23].

Gearbox

The TF2050 features an epicyclic gearbox with five planets. The planetary arrangement is chosen so that the fan and the IPC co-rotate. Also, for the same gear ratio, a star arrangement would be limited to four larger planets, making it a heavier design. Gear ratio and efficiency are kept constant and improved materials are anticipated for year 2050 [24].

Structural limits

Although matching procedures in PROOSIS use non-dimensional parameters, LPT rotational speeds have been calculated to check they do not exceed the AN2 criterion determined according to [25] at components' exit stage. The rim speed limits are 450 m/s for the HPT and 350 m/s for the LPT, allowing for material improvements. Flow areas have been calculated assuming low axial Mach numbers (0.22 and 0.4) and moderate exit hub-to-tip ratios (0.79 and 0.6) respectively for HPT and LPT, in order to maintain high component efficiencies.

Other components

Pressure losses in the ducts are kept constant. 50 kW is extracted from the HP spool to cover mechanical losses and power for the fuel pump, as in the year-2050 aircraft it is assumed that environmental control system (ECS) power is obtained from hydrogen fuel cells and not from the gas turbine engines.

These assumptions define the reference TF2050 engine, whose performance is detailed in Appendix B. The reference TF2050 reaches an OPR of approximately 75 and a turbine entry temperature (TET) of 1890 K at TOC, and an OPR of 62 at hot-day EOR conditions, where TET is limited to 1950 K.

YEAR-2050 TURBOFAN ENGINE SCALING STUDIES

The key parameters that affect the overall performance of the TF2050, quantified as total fuel burn for a given mission, are the specific fuel consumption, fan diameter and total engine weight. In order to assess their relative effects, nine scaled engines design point have been created, combining three TOC thrust levels (40, 46 and 55 kN), and three cruise bypass ratios (12.7, 16.7, 20.7). The scaling procedure has limited the compressor delivery temperature at cruise to 880 K, and the blade metal temperature of the first turbine rotor stage to 1400 K at EOR, to safeguard material integrity [26]. The remaining unknown parameters have been chosen by seeking the minimum cruise SFC. Additionally, HPC and HPT efficiencies have been reduced, to account for the effects of tip-leakage losses in the scaled-down cores, using the methods and equation described in [17]. Each design point follows a trade-off between reducing the OPR and accepting lower component efficiencies.

Figure 2 shows the cruise and TOC SFC, total engine weight and fan diameter for each configuration, normalized against the engine with a TOC thrust rating of 46 kN and a cruise bypass ratio (BPR) of 16.7. Second-order polynomial response surfaces are included to aid qualitative assessment of the results.

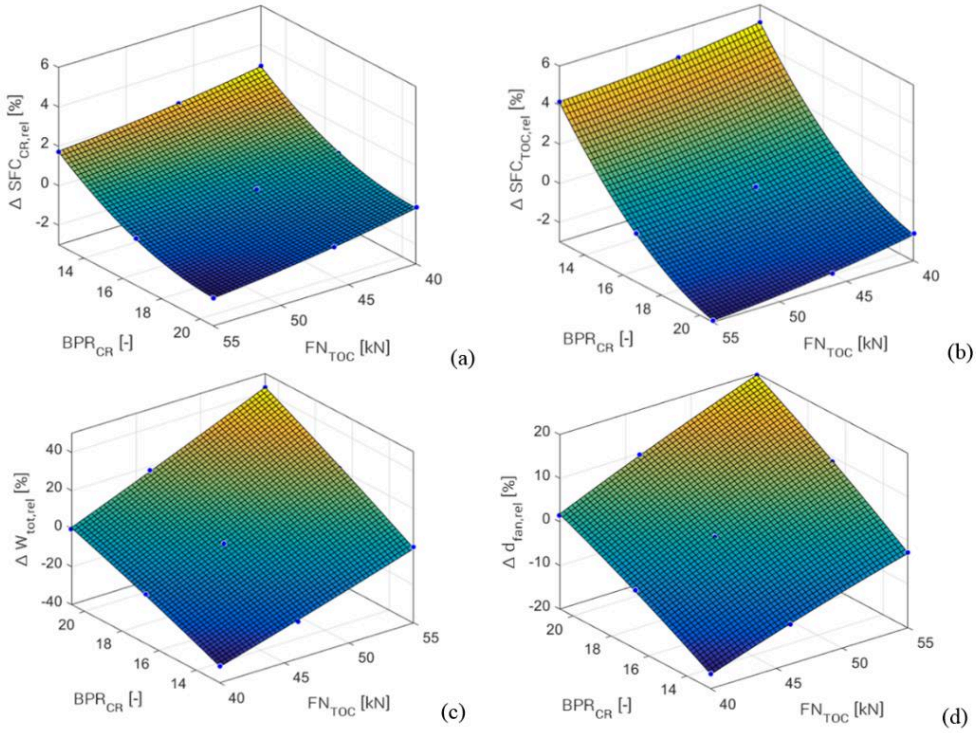

Figure 2: Trends of TF2050 scaling

Figures 2 a) and b) show that changes in bypass ratio affect the SFC more at TOC than at cruise. This is explained by the relatively-lower propulsive efficiency at TOC. This is not problematic, as cruise is the most influential contributor to mission fuel burn. According to Fig. 2 c) and d), fan diameter and engine weight both increase with BPR and TOC thrust. These trends oppose the SFC improvements and indicate the existence of an optimum bypass ratio for the lowest fuel-burn configuration, above which the weight and drag penalties outweigh the SFC reduction.

Appendix C offers more information on the performance of the nine study engines. An expected trend is the trade-off seen between OPR and HPC polytropic efficiency. At a fixed BPR, the maximum OPR decreases with reducing TOC thrust, due to the smaller, less-efficient, engine core components. Similarly, the OPR decreases at a fixed thrust level as BPR increases.

However, the engine producing 40 kN of thrust at TOC with a cruise bypass ratio of 20.7 is the only one to have an actual 'optimal' OPR, as the other eight are constrained by the limit on compressor delivery temperature. This explains the noticeable difference in OPR for the smallest-core engine relative to the trends shown by the others.

The lower HP pressure ratios of the lower-BPR engines are driven by the increase in optimal fan bypass pressure ratio (FPR) and the associated increase in fan core-section pressure ratios. The optimum FPR is primarily a function of BPR and increases with reducing BPR. This affects the HPC pressure ratio, because OPR is limited by the HPC delivery temperature and it appears preferable not to reduce work on the IPC as it has higher polytropic efficiency than the HPC.

Considering the three engines designed to deliver 55 kN at TOC, the total weight increase from the one with a cruise BPR of 12.7 to the one featuring BPR of 20.7 is over 2000 kg, with the fan diameter increasing by about 0.6 m. These considerable increases counteract the SFC improvements of about 4.6% at cruise and 8.3% at TOC. The engines feature different thrust levels at EOR and cruise at the specified TET levels because net

thrust at TOC was the only fixed thrust requirement. Trade-offs between thrust, TET and component life are possible at the other conditions.

FINAL TF2050 ENGINE

The final optimisation aims at identifying the most efficient engine/aircraft configuration for the intercontinental design mission using the scaling study. The reference aircraft design, some engine performance and the trade factors are specified in [13, 26], with an approach similar to the one in [27].

Two sets of fuel-burn trade factors are defined: linear trade factors (LTF), and non-linear trade factors (NLTF). Each trade factor converts a different key performance parameter (weighted SFC, total engine weight or fan diameter) into a change in mission fuel burn, thus enabling a common metric for engine evaluation. Table 1 presents the values adopted for the trade factors. The trade factor for SFC uses a combination of cruise, TOC and EOR values against their reference as in Appendix B, where the contribution of each depends on the amount of fuel burned at the respective condition. For the 7000 NM case, the cruise contribution is 92.9%, TOC accounts for 6.1% and the remaining 1% is attributed to EOR, as shown in Eq.1. Equation 2 describes the formulation used for fuel burn variations.

Key parameter	Mission FB variation
+1 % SFC_{we}	+1.51 % FB
+500 kg total engine weight	+1.03 % FB
+1 % fan diameter	+0.16 % FB

Table 1: Linear trade factors for TF2050

$$\Delta \mathrm{SFC}_{\mathrm{we}} = 0.061\left(\frac{\mathrm{SFC}_{\mathrm{TOC}}}{\mathrm{SFC}_{\mathrm{TOC,ref}}} - 1\right) + 0.029\left(\frac{\mathrm{SFC}_{\mathrm{cr}}}{\mathrm{SFC}_{\mathrm{cr,ref}}} - 1\right) + 0.01 \cdot \left(\frac{\mathrm{SFC}_{\mathrm{EOR}}}{\mathrm{SFC}_{\mathrm{EOR,ref}}} - 1\right) \quad (1)$$

$$\Delta FB = 1.51 \cdot 100\, \Delta SFC_{we} + 1.03 \cdot 100 \frac{(W - W_{ref})}{500} + 0.016 \cdot 100\left(\frac{d_{fan}}{d_{fan,ref}} - 1\right) \quad (2)$$

Whilst LTFs are valid only for relatively small deviation from initial design point, NLTFs are more precise for larger variations of input parameters, but their use involves an iterative procedure. NLTFs have been summarized in graphic format and presented in [13] for both the long-range and short-range platforms. For NLTFs, the PROOSIS engine models provide weighted SFC from assumed thrust levels and performance requirements. Then, WeiCo determines fan diameter and weight, hence mission fuel burn is calculated. Variations in engine weight and total fuel consumed imply the recalibration of design thrust levels, so successive sizing loops are required until engine performance requirements and engine layout reach convergence.

Given the range of variation between the original reference engine and the results of an initial LTF-based optimisation, NLTFs have been used for the final optimisation of the TF2050.

The final TF2050 has a cruise BPR of 16.84 and a maximum OPR of 75.4 at TOC. Coupled with the re-sized year-2050 ATW aircraft, it burns $47.5 \cdot 10^3$ kg of fuel for a 7000 NM mission. Hence, it offers a mission fuel burn reduction of about 46% per available seat kilometer (ASK) relative to the Trent 772-like baseline engine model on the year-2000 aircraft. The optimisation itself reduces the mission fuel burn by 1.59% compared

with the original reference engine. Table 2 presents some general performance data, while detailed figures are given in Appendix D.

Parameter	Units	cruise	TOC	EOR
Mach no.	-	0.80	0.82	0.20
Altitude	m	11277	10668	0
dT ISA	K	0	+10	+15
HP shaft mech. losses	kW	50	50	50
IP shaft mech. losses	kW	50	50	50
Total net thrust	kN	32.56	49.99	183.46
BPR	-	16.84	16.08	16.14
OPR	-	62.1	75.4	60.13
TET	K	1540	1890	1921
Thermal efficiency	-	0.53	0.54	0.46
Propulsive efficiency	-	0.82	0.78	0.42
Overall efficiency	-	0.44	0.42	0.20
Specific thrust	m/s	84.6	111.3	1883.1
Air mass flow	kg/s	384.7	449.0	1002.2
SFC	g/kN.s	12.60	13.73	8.28
Total engine weight	kg	5161.3		
Fan diameter	m	2.840		
Reduction Gear Ratio	-	4.3		

Table 2: Summary data for TF2050

When comparing data for the final TF2050 engine with the baseline from Appendix A, several differences stand out. First, the net thrust rating has been reduced by 37.9% at cruise and by 31.5% at TOC, due to a more-aerodynamic and lighter aircraft and more fuel-efficient engines. This is despite an assumed 8.3% increase in the number of seats and a 44% increase in design range. TOC thrusts also reduce because of a 'cascading effect'. Lower SFC leads to reduced block fuel weight, which enables the resizing of structures, such as wings and landing gear, giving more weight savings resulting in lower thrusts etc.

The cruise SFC is 12.60 g/kN.s, which is a reduction of 26.8% from the year-2000 baseline. The improvement is partly due to the higher cruise altitude and lower Mach number, but it mostly derives from the improvement in thermodynamic cycle efficiency

and a 12% increase in propulsive efficiency, related to the higher bypass ratio, which is more than tripled from the year-2000 engine. Another contributor is the reduction in HP shaft power offtake from 310 kW to 50 kW, since the ECS power demand is assumed to be met by hydrogen fuel cells instead of being taken from the main engines. Thermodynamic cycle efficiency is favored by turbine entry temperatures being raised by more than 200 K, reaching over 1900 K at EOR hot-day take-off. This is enabled by materials improvements and effective cooling techniques that limit peak blade metal temperature to 1400 K. Another factor is the significant increase in overall pressure ratio, which reaches 62.1 at cruise and 75.4 at TOC, with an increase of 62% in the latter case with respect to the baseline. The optimized BPR is lower and the specific thrust is higher than the originally proposed reference engine values, while the optimum OPR is slightly lower. This is explained by the trends in weight and diameter for the scaled-down engine, as presented in Fig. 2 c) and d), by the different work split of the components, and by the penalty in turbomachinery efficiency for the smaller last-stage compressor blade height resulting from the high OPR and reduced core mass flow.

Relative to the year-2000 baseline engine, the inlet mass flow of the optimized engine still increases by about 7% at cruise and 17% at TOC, despite the lower thrust requirement. This compensates for the reduced fan pressure ratio and specific thrust, and it entails a fan diameter increase of 36 cm. However, the lower thrust requirements and improvements in materials and design help reduce the final TF2050 engine weight to 5161 kg, a 35% saving compared to the baseline engine. It is also a significant

reduction in respect to the 5528 kg of the original reference engine, resulting from the scaling and use of the NLTFs.

The optimisation reduces the fuel burn by 1.6%. It does not cause an actual reduction of SFC, as the difference from value in Appendix B is due to different flight condition; the effects of improved technologies and core reduction almost cancel out. This is shown in the SFC loops for two cruise Mach numbers and altitudes presented in Fig.3. The fuel burn benefit stems from the improved airframe aerodynamic and the engine weight and drag reduction.

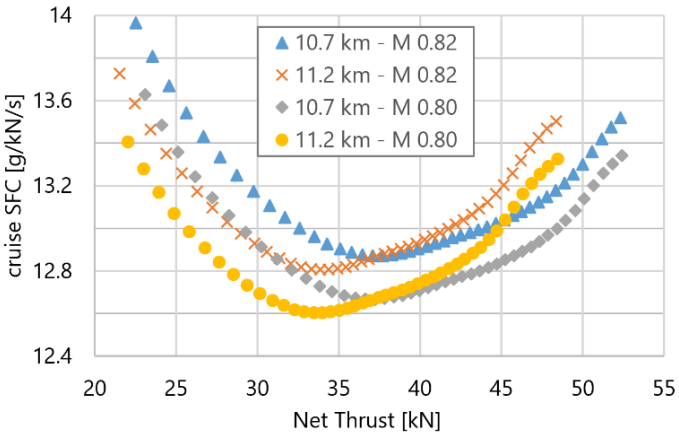

Figure 3: cruise SFC loops for TF2050

GOR2050 OUTLINE AND MODELLING ASSUMPTIONS

The envisaged aircraft design for short to mid-range missions in year 2050 features a geared open rotor in pusher configuration [28], where a high speed LPT powers the propeller array through an epicyclic reduction gearbox, as represented in Fig. 4. Similar to the TF2050, innovations in aircraft design and manufacturing are claimed to significantly reduce the drag while increasing the payload and range

capability over the year-2025 baseline aircraft [13]. The passenger number for the aircraft has been increased from 150 to 180.

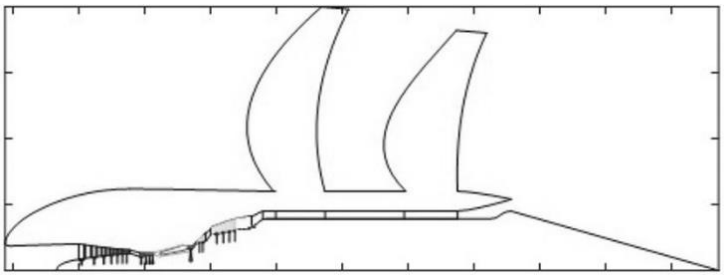

Figure 4: Schematic configuration of GOR2050

As the powerplant architecture differs radically from the baseline engine, a direct comparison is more difficult. A GOR design, proposed for entry into service by 2025, is utilized to benchmark the reference GOR2050 [29]. Slight improvements in efficiency and pressure ratio are registered.

The conventional elements follow the criteria presented for the TF2050 for turbomachinery components, ducts, nozzles, compressor delivery temperature and structural limits. The pressure losses in the combustor are 4%. The selection of a GOR introduces novel components that are not present in existing aircraft: they are modelled ex-novo in PROOSIS as follows.

Contra-rotating propellers (CRP)

There are several methodologies to capture the performance of a CRP array [30-36], which is a key component for the GOR2050. However, due to a balance between fidelity and computational cost involved, a 1D methodology has been adopted. Full details are available in [36].

The methodology couples a blade element method approach [37] and a stream-tube contraction approach based on momentum models [38]. Each propeller is assumed to work on the flow field generated by the flight speed, and the effects of the other propeller, called induced velocity. Each propeller also produces a self-induced velocity, corresponding to the change in velocity produced by the operation of the single propeller (Fig. 5, where axial and tangential induced components are shown). As the induced velocities are oscillating, their time-averaged magnitude is considered [39-44]. A scaled map from the SR-7 propeller [45] is adopted for off-design performance of each propeller. The efficiency value is corrected to include effects of loading, number of blades and technology improvements, as the experimental data refer to 1980s technology [36, 45]. The rear propeller blade height is clipped by 20% compared to the front propeller to reduce noise levels during low speed operation [36].

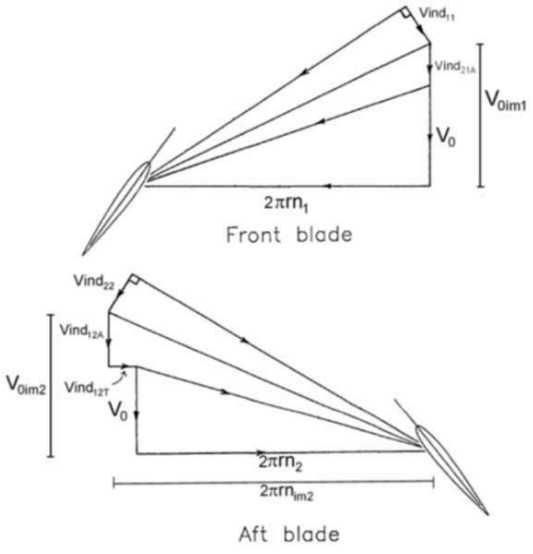

Figure 5: Schematic configuration of the GOR2050

It is also assumed that pylon blowing for noise attenuation purposes [46] will feature in rear-fuselage installed GOR engine designs. A methodology derived from NASA [47] has

been introduced to account for the performance implications of such a system, as illustrated in Fig. 6. Pylon blowing is supposed to activate if the flow deflection at 75% of the span exceeds 40° and the imaginary advance ratio Jim (the advance ratio increased to consider induced velocity) is higher than 1.2. Its activation suddenly increases the angle of attack of the propeller blades; hence the thrust coefficient is increased through the percentage correction presented in Eq. 3. The pylon blowing system is supposed to be powered by the fuel cells, with no impact on main engine power offtake.

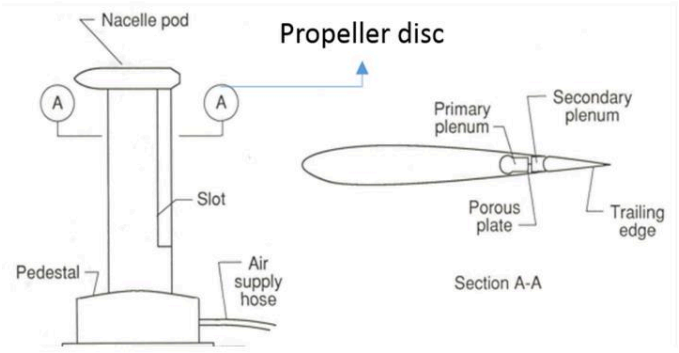

Figure 6: Schematic of pylon blowing arrangement, adapted from [47]

The performance of the CRP can be estimated via an iterative process. An important modelling supposition is that the CRP rotates at fixed rotational speed while a pitch control mechanism (PCM) varies the pitch angle to obtain the desired gross thrust. In practice, changes in rotational speed are expected for noise attenuation during low speed operations.

$$\delta_{ct} = 2.6863\, J_{im}{}^{2} - \ 1.0988\, J_{im} - \ 2.5117 \tag{3}$$

Differential Planetary Gearbox (DPGB)

The DPGB is considered to be an inline epicyclic gear train in a differential arrangement [48]. The sun gear is connected to the LP turbine shaft, while the ring and carrier are connected to the forward and rear propellers respectively. Equations 4-7 characterize the design-point performance of the DPGB [49]. The torque ratio (TR) is defined as the ratio between the carrier and the ring torque. It dictates the ratio of the radii of the planet gears compared to the sun gear (k). Operational speeds of the ring (N_{ring}) and carrier ($N_{carrier}$) and the gear ratio establish the speed of the sun gear (N_{sun}). A torque (Q) balance yields the available power to the forward and rear propellers for a given mechanical transfer efficiency.

The off-design operation of the DPGB is characterized by the map in Fig. 7 [50]. The mechanical efficiency of DPGB is expressed as function of the non-dimensional input torque and rotational speed. The variation in the mechanical transmission efficiency leads to a variation in the steady-state heat rejection (HR) of the DPGB, proportional to the power (Pw_{sun}) transmitted from the LPT through the sun gear as per Eq. 8.

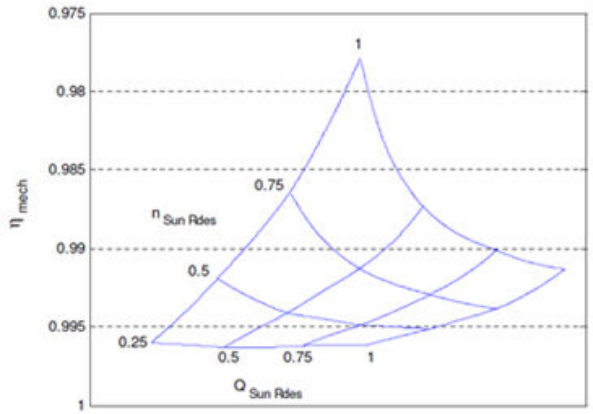

Figure 7, DPGB map, adapted from [50]

Additional components

An independent air-oil cooling system is introduced for the DPGB, due to its significant heat generation [36]. For simplicity of calculations, it is modelled with an axial 'blower' compressor fed by ambient air, a cross-flow air-oil heat exchanger, and a scoop nozzle. The blower activates below Mach 0.35 with an assumed 88% efficiency. The heat exchanger rejects heat to reduce oil temperature according to a simple balance defined in Eq. 9. Cooling effectiveness and pressure drop are assumed as constant. The thrust contribution of the cooling air is negligible apart from the EOR take-off condition, where it represents 1.7% of the overall thrust.

The rotating blade roots of the CRP array pass radially through the annular duct between the LPT and the core nozzle. The consequent total pressure loss in the duct crossing the cascade is determined in Eq. 10-11 as a function of the flow deflection (assuming that the velocity triangles of the CRP at 75% span are the same as at the root), and the aspect ratio of the cascade [51]. The work transferred by exhaust gases to CRP is considered negligible.

No bleed is extracted for ECS requirements. A power offtake of 77.5 kW from the HP spool of each engine suffices for seal windage and inefficiencies, bearing losses, mechanical losses, the PCM and the fuel and oil pumps.

$$\mathrm{k} = 2 - [TR/(2TR - 2)] = R_{carrier}/R_{sun} \tag{4}$$

$$N_{sun} = N_{ring}(1 + 2k) + N_{carrier} \cdot 2(1 + k) \tag{5}$$

$$-Q_{ring} = Q_{sun}(1 + 2k)\eta_{mech} \tag{6}$$

$$-Q_{carrier} = 2Q_{sun}(1 + k)\eta_{mech} \tag{7}$$

$$HR_{DPGB} = Pw_{sun}(1 - \eta_{mech}) \quad (8)$$

$$HR_{DPGB} = \dot{m}_{cool} c_p (\Delta T_{cool}) \varepsilon_{cool} \quad (9)$$

$$\xi_p = 0.025[1 + 2(\beta/90°)] \quad (10)$$

$$\xi_{total} = \xi_p[1 + 3.2(b/h)] \quad (11)$$

GOR SCALING STUDIES

A similar scaling study to that described for the TF2050 has been performed for GOR2050. Three TOC thrust levels have been defined namely 18, 22.2 and 25 kN [50]. The scaling study assumes no changes in duct and combustor pressure losses, pressure ratio split, propeller loading at TOC, cooling flow bleed percentages or turbomachinery efficiency. The TET at TOC can range between 1700 K and 1750 K. Polytropic and isentropic efficiencies of IPC, IPT and LPT are retained, while the polytropic efficiency of the HPC is altered through Eq. 12, as a function of the compressor last-stage blade height. The reference engine features a blade height h_{ref} = 12.25 mm, with an exit Mach number of 0.25 and hub-to-tip ratio of 0.895. The correction for HPT polytropic efficiency is again half of the value for the HPC [27, 52].

$$\delta_{poly,HPC} = 0.056977 - 0.5547h - 1.7724h^{-2} \quad (12)$$

Based on scaling results, some notable design-point trends can be observed. Fig. 8 indicates that, as the TOC thrust level increases, the engine SFC reduces. This benefit comes from the increased last-stage blade height (LSBH) in the HPC, which also favors the OPR increase with net thrust. The increase of dry weight with thrust level is also

shown. It is explained by the increase in propeller size, as the propeller loading is kept fixed, and by the effect on the supporting rotating structures. Appendix E provides numerical details from the scaling exercise.

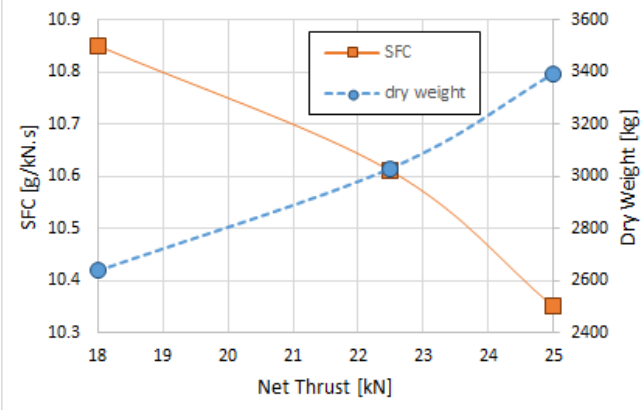

Figure 8: Notable trends for GOR2050 scaling study

FINAL GOR2050 ENGINE

The latest aircraft configuration [13] is such that the engine thrust requirement is 17.34 kN at TOC, falling outside of the range considered in the scaling study. The cruise altitude is increased to 11.277 km. As a consequence, the design point values are extrapolated from the previous figures. For the final optimisation, the linear trade factors in Tab. 3 have been used to produce the final set of performance parameters, as shown in Eq. 13-14 [26]. Linear trade factors only are used because of the small deviation from the original reference engine. The weightings for calculating ΔSFC_{we} differ from the values in Eq.1 and 2 for TF2050, as the design mission range is shorter. The final GOR2050 features are shown in Tab. 4. The TET has been limited to 1950 K at EOR for hot-day take-off and below 1650 K at cruise to preserve blade life.

Key parameter	Mission FB variation
+ 1 % SFC_{we}	+ 1.15 % FB
+ 500 kg total engine weight	+ 2.01 % FB

Table 3: linear trade factors for GOR2050

Figure 9 shows the discrepancies in the trends of the design-point core flows and SFCs as a function of design-point thrusts. The variation from extrapolating trends is shown, in both a quadratic and a linear manner. The new design point SFC deviates from the projected SFCs because the forward propeller diameter is specified. As a consequence, the forward propeller loading decreases and so does the CRP operational rotational speed at TOC conditions, in both cases by about 18% when compared to the 18 kN design. The combined reductions in propeller loading and tip speed lead to an increase in net propeller efficiency and a decrease in the SFC and core mass flow at design-point conditions. The reduced core mass flow again reduces the last stage blade height, whose detrimental effect on efficiency drives the preferred configuration towards a lower OPR cycle.

The final scaled GOR2050 provides a mission fuel burn of $9.37 \cdot 10^3$ kg for 3500 NM, improved by 59% versus the year 2000 value per passenger kilometer.

Parameter	Units	GOR2050			GOR2025
		TOC	cruise	EOR	cruise
Mach no.	-	0.73	0.71	0.2	0.75
Altitude	m	10668	11277	0	11277
dT ISA	K	10	0	15	0
Net Thrust	kN	17.34	13.85	78.95	16.7
OPR	-	41.1	36.8	33.4	48.4
TET	K	1750	1628	1950	1714
Core air mass flow	kg/s	7.08	6.17	17.43	-
SFC	g/kN.s	10.75	10.41	6.44	11.87
Forward Propeller d	m	4.0	4.0	4.0	4.27
Rear Propeller d	m	3.5	3.5	3.5	3.73

Table 4: summary data for final GOR2050 and GOR2025

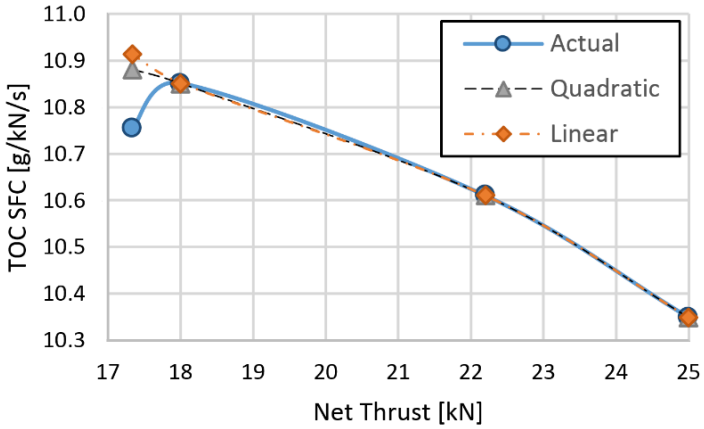

Figure 9: TOC SFC trends for GOR2050

The design point SFC reduces by 39% compared to its baseline and by 9.5% compared to the GOR2025 specifications. The OPR decreases from 48.4 to 41.1, because of the last stage blade height penalty. The optimisation reduces the thrust requirement by 7% compared to reference, whilst the increase against the value for the GOR2025 is 8%, due to the increased payload.

Table 4 also include specified cruise parameter of a 2025 entry-into-service open-rotor for benchmark. The optimisation reduced OPR and thrust rating, as the propeller size decrease to reduce the weight of the engine. This accumulates a 12% SFC cruise benefit in favor of the GOR2050. The optimization of the design-point SFC is mainly driven by the efficiency of the CRP array. Net efficiency of the CRP is dictated more by the advance ratio, at relatively higher Mach numbers, than by the swirl recovery of the rear propeller.

The weight of the final GOR2050 engine is mainly driven by the CRP array and the DPGB, which respectively account for 54% and 15% of the total mass. Performance details are included in Appendix F.

CONCLUSIONS

This paper has presented modelling assumptions and results for year-2050 study engines for short to medium and long-range commercial aircraft. The potential performance improvements from evolved component designs and novel components for a geared turbofan and a geared open rotor have been presented. Scaling studies have helped to understand trade-offs between specific fuel consumption, fan diameter and weight following changes in engine thrust levels to suit matching evolved advanced tube-and-wing aircraft designs. Optimisation studies minimizing mission fuel burn and CO_2 emissions have provided definitive reference engine designs and performance data.

Starting with these models, further optimisation studies are possible, like a trade-off between maximum cycle temperature and turbine blade life, or economic analyses to assess the viability and relative profitability of the engine concepts. The applied cycle constraints mean that high engine noise and NO_x emissions are avoided, but those attributes are not part of the objective functions in the reported studies.

These engines serve as benchmarks for the assessment of more complex cycles integrating novel technologies such as intercooling and recuperation, topping and bottoming cycles, secondary combustion, cryo-fuels and electrification that are likely to be developed in the mid-century timeframe.

ACKNOWLEDGMENT

The authors would like to thank Dr. Vishal Sethi, Dr. Devaiah Nalianda from Cranfield University and other ULTIMATE project partners for their support.

FUNDING

This project has received funding from the European Union's Horizon 2020 research and innovation programme under Grant Agreement No. 633436.

NOMENCLATURE

ASK	available seat per kilometer
ATW	advanced tube and wing (aircraft)
BPR	bypass ratio
CMC	ceramic matrix composites
CRP	contra-rotating propellers
Ct	propeller thrust coefficient
C_x	nozzle thrust coefficient
DPGB	differential planetary gearbox
ECS	environmental control system
EOR	end of runway
FB	fuel burn
FN	net thrust
FPR	fan pressure ratio
GOR	geared open rotor
HPC	high pressure compressor
HPT	high pressure turbine
HR	heating power released
IPC	intermediate pressure compressor

IPT	intermediate pressure turbine
ISA	international standard atmosphere
J	propeller advance ratio
LPT	low pressure turbine
LSBH	last stage blade height
LTF	linear trade factor
LTO	landing and take-off
M	Mach number
N	rotational speed
NLTF	non-linear trade factor
NM	nautical mile
OPR	overall pressure ratio
PCM	pitch control mechanism
PR	pressure ratio
Pw	mechanical power
Q	torque
R	radius
RPK	Revenue per passenger kilometer
SFC	specific fuel consumption

T	temperature
TET	turbine entry temperature
TOC	top of climb
TR	torque ratio
TRL	technology readiness level
V	velocity
W	weight
b	blade span
cp	specific heat at constant pressure
d	diameter
h	blade height
k	ratio of carrier and sun radii for DPGB
$\dot{m}$	mass flow

Greek

β	deflection angle
δ	thrust coefficient conversion
ε	cooling effectiveness
η	efficiency

ξ	pressure loss factor

Subscripts

ax	axial
cool	coolant
ind	induced velocity
is	isentropic
o	flight velocity
mech	mechanical
p	profile
poly	polytropic
ref	relative to reference
we	weighted

REFERENCES

[1] “Leading airlines worldwide in 2018, by passenger kilometers flown”, statista.com, https://www.statista.com/statistics/270986/airlines-by-passenger-kilometers-flown (accessed January 15, 2019)

[2] ICAO Economic Development Air Transport Bureau, “State of Global Air Transport and ICAO Forecasts for Effective Planning”, ICAO, https://www.icao.int/Meetings/ICAN2017/Documents/ICAO%20Workshop%20-%20State%20of%20Industry%20and%20ICAO%20Forecasts.pdf (accessed January 15, 2019)

[3] Boeing, “Current Market outlook 2016-2035”, Boeing Company, http://www.boeing.com/resources/boeingdotcom/commercial/about-our-market/assets/downloads/cmo_print_2016_final.pdf (accessed January 15, 2019)

[4] ACARE, 2017, “Strategic Research & Innovation Agenda, Volume 1, Delivering Europe’s Vision for Aviation”, Advisory Council for Aviation Research and Innovation in Europe, https://www.acare4europe.org/sites/acare4europe.org/files/document/ACARE-Strategic-Research-Innovation-Volume-1.pdf (accessed January 15, 2019)

[5] Reneaux, J., 2004, “Overview on Drag Reduction Technologies for Civil Transport Aircraft”, *European Congress on Computational Methods in Applied Sciences and Engineering - ECCOMAS 2004,* Jyväskylä, Finland

[6] Gundlach, J.F, *et al.*, 2000, “Conceptual Design Studies of a Strut-Braced Wing Transonic Transport”, Journal of Aircraft, **37**(6), pp.976-983. DOI: 10.2514/2.2724

[7] Bradley, M. K., Droney, C. K., 2011, “Subsonic Ultra Green Aircraft Research: Phase I Final Report”, Technical Report No. CR-2011-216847, NASA Langley Research Center, Hampton, VI

[8] Liebeck, R. H., 2004, “Design of the Blended Wing Body Subsonic Transport”, Journal of Aircraft, **41**(1), pp. 10-25, DOI: 10.2514/1.9084

[9] Felder, J. L., Kim, H. D., Brown, G. V., 2009, “Turboelectric Distributed Propulsion Engine Cycle Analysis for Hybrid-Wing-Body Aircraft”, *47th AIAA Aerospace Sciences Meeting including The New Horizons Forum and Aerospace Exposition*, Orlando, FL. DOI: 10.2514/6.2009-1132

[10] Poel, H. W., Malychev, V. V, 1997, “Hydrogen in Future Civil Aviation”, International Journal of Hydrogen Energy, **22**(10-11), pp. 1061-1069, DOI: 10.1016/S0360-3199(95)00140-9

[11] Rolt, A., Kyprianidis, K., 2010, "Assessment of New Aeroengine Core Concepts and Technologies in the EU Framework 6 NEWAC Programme", *Proc. 27th Congress of the International Council of the Aeronautical Sciences* **4**, pp. 2736-2746, Nice, France.

[12] Gronsted, T., *et al.*, 2016, "Ultra Low Emission Technology Innovations for Mid-century Aircraft Turbine Engines", *Proc. ASME Turbo Expo 2016: Turbomachinery Technical Conference and Exposition*, Seoul, South Korea. DOI: 10.1115/GT2016-56123

[13] Heinemann, P., *et al.*, 2017, "Advanced Tube and Wing Aircraft for Year 2050 Timeframe", *55th AIAA Aerospace Sciences Meeting*, Grapevine, TX. DOI: 10.2514/6.2017-1390

[14] Alexiou, A., Tsalavoutas, T., 2011, *Introduction to Gas Turbine Modelling with PROOSIS – First Edition*, Empresarios Agrupados International, Madrid, Spain

[15] Rolls-Royce, 2016, "Rolls-Royce Trent 700 poster", Rolls Royce plc. https://www.rolls-royce.com/~/media/Files/R/Rolls-Royce/documents/civil-aerospace-downloads/High-Res-posters/High-Res-poster-Trent-700.pdf (accessed January 15, 2019)

[16] EASA, 2018, "Type-Certificate Data Sheet No. E.067 for CFM56-5 series engines" EASA. https://www.easa.europa.eu/sites/default/files/dfu/EASA%20TCDS%20E.067_issue%2002_20180417.pdf (accessed January 15, 2019)

[17] Rolt, A., *et al.*, 2017, "Scale effects on conventional and intercooled turbofan engine performance", The Aeronautical Journal, **121**(1242) pp. 1162-1185. DOI: 10.1017/aer.2017.38

[18] Cumpsty, N. A., 2015, *Jet Propulsion: A simple guide to the Aerodynamic and Thermodynamic Design and Performance of Jet Engines*, *3th ed*., Cambridge University Press, Cambridge, UK, DOI: 10.1017/CBO9781316223116

[19] Cornell, W. G., 1975, "Experimental Quiet Engine Program - Summary Report," Contractor Report No. CR-2519, NASA Lewis Research Center, Cleveland, OH

[20] Converse, G. L, Griffin R. G., 1984, "Extended Parametric Representation of Compressor Fans and Turbines- Volume 1", Contractor report No. CR-174645, NASA Lewis Research Center, Cleveland, OH

[21] Plencer, R. M., 1989, "Plotting Component Maps in the Navy/NASA Engine Program (NNEP) - A Method and its Usage", Technical Report No. TM-101433, NASA Lewis Research Center, Cleveland, OH

[22] Stabe, R. G., Whitney, W. J., and T. P. Mofitt, T.P., 1984, “Performance of a High-Work Low Aspect Ratio Turbine Tested with a Realistic Inlet Radial Temperature Profile”, *Proc. AIAA/SAE/ASME 20th Joint Propulsion Conference*, Cincinnati, OH. DOI: 10.2514/6.1984-1161

[23] Serovy, G. K., 1976, “Compressor and Turbine Prediction System Development - Lessons from Thirty Years of History”, AGARD Lecture Series No. 83 on Modern Prediction Methods for Turbomachine Performance.

[24] ANSI, AGMA, 2006, *Design Manual for enclosed epicyclic gear drives*, American Gear Manufacturers Association, Series ANSI/AGMA 613-B06, ISBN: 978-1555898755

[25] Walsh, P. P., Fletcher, P., 2004, *Gas Turbine Performance - 2nd Edition*, Blackwell Publishing, Oxford, UK. ISBN: 978-0632064342

[26] Heinemann, P., Kaiser, S., 2016, “ULTIMATE MS2: Advanced Tube and Wing Trade Factors provided to WP1”, Internal report (confidential)

[27] Kyprianidis, K., Rolt, A., 2014, “On the Optimisation of a Geared Fan Intercooled Core Engine Design”, ASME J. Eng. Gas Turbines Power, **137**(4), pp. 041201. DOI: 10.1115/1.4028544

[28] Parker, R., 2014, “Large civil aircraft engines for the future – Evolution and revolution”, General Lecture 1, ICAS-201-0.2, St. Petersburg, Russia. https://www.icas.org/media/pdf/ICAS%20Congress%20General%20Lectures/2014/Parker.pdf

[29] Newton, P., *et al*., 2015, “ULTIMATE D1.1 - Establish Common Year 2050 Technology Level Assumptions”, Internal report (confidential)

[30] Laban, M., Kok, J. C., Prananta, B. B., 2010, "Numerical tools for contra-rotating open rotor performance, noise and vibration assessment", *Proc. 27th Congress International Council of the Aeronautical Sciences*, Nice, France.

[31] Wald, Q. R., 2006, "The aerodynamics of propellers", Progress in Aerospace Sciences, **42**(2), pp. 85-128. DOI: 10.1016/j.paerosci.2006.04.001

[32] Gur, O., Rosen, A., 2008, "Comparison between blade-element models of propellers", The Aeronautical Journal, **112**(1138), pp. 689-704. DOI: 10.1017/S0001924000002669

[33] Egolf, T.A., *et al*., 1988, "An Analysis for High Speed Propeller-Nacelle Aerodynamic Performance Prediction, Volume I – Theory and Application", Contractor Report No. CR-4199, NASA Lewis Research Center, Cleveland, OH

[34] Korkan, K. D., Gregorek, G. M., Mikkelson, D.C., 1980, "A Theoretical and Experimental Investigation of Propeller Performance Methodologies", *Proc. AIAA/SAE/ASME 16th Joint Propulsion Conference*, Hartford, CT. DOI: 10.2514/6.1980-1240

[35] Bocci, A. J., Morrison, J. I., 1985, "A review of ARA research into propeller aerodynamic prediction methods", *AGARD Conference Proceedings No. 366, Aerodynamics and Acoustics of Propellers*

[36] Bellocq, P., 2012, "Multi-Disciplinary Preliminary Design Assessments of Pusher Counter-Rotating Open Rotors for Civil Aviation", PhD Thesis, Cranfield University, UK

[37] Nelson, W. C., 1944, *Airplane propeller principles*, J. Wiley & Sons, Inc., New York, NY; Chapman & Hall, Ltd., London, UK

[38] Chandrasekaran, B., 1985, "Method for the prediction of the installation aerodynamics of a propfan at subsonic speeds", Contractor Report No. CR-3887, NASA Langley Research Center, Hampton, VI

[39] Lock, C. N. H., 1941,"Interference velocity for a close pair of contra-rotating airscrews", *Aeronautical Research Council Reports and Memoranda*, Reports and Memoranda No. 2084, London, UK

[40] Denner, B. W., Korkan, K. D., 1990, "An Approximate Model for the Performance and Acoustic Predictions of Counterrotating Propeller Configurations", *AIAA 28th Aerospace Sciences Meeting*, Reno, NV. DOI: 10.2514/6.1990-282

[41] Playle, S. C., Korkan, K. D., Von Lavante, E., 1986, "A numerical method for the design and analysis of counter-rotating propellers", Journal of Propulsion, **2**(1), pp. 57-63. DOI: 10.2514/3.22845

[42] Ginzel, F., 1949, "Calculation of counterrotating propellers", Technical Report No. TM-1208, NACA, Washington, DC

[43] Davidson, R. E., 1981, "Optimization and performance calculation of dual rotation propellers", Technical Report No. TP-1948, NASA Langley Research Center, Hampton, VI

[44] Naiman, I., 1943, "Method of Calculating Performance of Dual-rotating Propellers from Airfoil Characteristics", Wartime Report No. WR-L-330, NACA, Washington, DC

[45] Mikkelson, D. C., Mitchell, G. A., Bober, L., J., 1984, “Summary of Recent NASA Propeller Research,” Technical Report No. TM-83733, NASA Lewis Research Center, Cleveland, OH

[46] Sinnige, T., Veldhuis, L. L., 2014, "Pylon trailing edge blowing effects on the performance and noise production of a pusher propeller", *Proc. 52nd Aerospace Sciences Meeting, AIAA SciTech Forum*, National Harbor, MD. DOI: 10.2514/6.2014-0566

[47] Gentry, G. L., Booth, E. R., Takallu, M. A., 1990, “Effect of Pylon Wake with and Without Pylon Blowing on Propeller Thrust”. Technical Report No. TM-4162, NASA Langley Research Center, Hampton, VI

[48] Lynwander, P., 1983, *Gear Drive Systems: Design and Application*, CRC Press, Boca Raton, FL. ISBN: 978-0824718961. DOI: 10.1201/9780203755075

[49] Dooner, D. B., 2012, *Kinematic Geometry of Gearing*, *Second Edition*, John Wiley & Sons Ltd, New York, NY, ISBN: 978-1119950943. DOI: 10.1002/9781119942474

[50] Dominy, J., “Transmission Efficiency in Advanced Aerospace Powerplant”, *Proc. AIAA/SAE/ASME/ASEE 23rd Joint Propulsion Conference*, Cincinnati, OH

[51] Horlock, J. H., 1966, *Axial Flow Turbines: Fluid Mechanics and Thermodynamics*, Butterworths, London, 1966

[52] Mattingly, J. D., Heiser, W. H., Pratt, D. T., 2002, *Aircraft Engine Design, Second Edition*, AIAA Education Series, Washington, DC. ISBN: 978-1563475382. DOI: 10.2514/4.861444

APPENDIX A

Parameter	Units	LR2000			SR2000		
		TOC	cruise	EOR	TOC	cruise	EOR
Altitude	m	10668	10668	0	10668	10668	0
Mach number	-	0.82	0.82	0.25	0.82	0.82	0.25
Delta from ISA	K	+10	0	+15	+10	0	+15
Net thrust	kN	73.0	52.4	251.0	30.1	21.9	96.1
Bypass Ratio	-	4.7	5.2	5.1	4.6	5.1	5.1
OPR	-	46.5	36.5	39.2	35.7	28.4	28.2
TET	K	1691	1422	1757	1530	1357	1599
SFC	g/kN.s	18.6	17.3	13.0	18.9	18.0	14.0
Inlet mass flow	kg/s	381.8	358.8	939.0	150.7	140.9	372.0
Engine weight	kg	7972 (total)			3086 (total)		
Fan diameter	m	2.474			1.735		
Mission fuel burn	kg	$86.4 \cdot 10^3$			$22.9 \cdot 10^3$		

Table 5: Summary of baseline year-2000 engines

APPENDIX B

Component	Parameter	Units	cruise	TOC	EOR
General	Mach	-	0.82	0.82	0.25
	Altitude	km	10.7	10.7	0
	dT ISA	K	0	+10	+15
	HP shaft power offtake	kW	260	260	260
	HP shaft mech. losses	kW	50	50	50
	IP shaft mech. losses	kW	50	50	50
	Total net thrust	kN	49.0	65.4	239.2
	BPR	-	20.1	19.6	18.9
	OPR	-	64.4	75.2	61.9
	Gearbox efficiency	-	0.995	0.995	0.995
Output	Thermal efficiency	-	0.527	0.531	0.451
	Propulsive efficiency	-	0.837	0.809	0.523
	Specific thrust	m/s	72	93.1	152.3
	Engine air mass flow	kg/s	680.6	702.7	1570.6
	SFC	g/kN.s	12.88	13.52	8.65

Table 6: Summary of reference TF2050

APPENDIX C

TOC FN	**Units**	**55**	**55**	**55**	**46**	**46**	**46**	**40**	**40**	**40**
Cruise BPR		**20.7**	**16.7**	**12.7**	**20.7**	**16.7**	**12.7**	**20.7**	**16.7**	**12.7**
Cruise FPR_{BP}	-	1.33	1.40	1.53	1.33	1.40	1.53	1.33	1.40	1.52
Cruise IPC PR	-	2.64	2.64	2.62	2.62	2.62	2.56	2.56	2.62	2.59
Cruise HPC PR	-	19.72	18.91	17.88	19.51	18.89	18.07	18.62	18.69	17.67
HPC η_{poly}	-	0.909	0.910	0.910	0.906	0.906	0.906	0.903	0.902	0.903
HPC η_{is}	-	0.869	0.870	0.871	0.863	0.864	0.865	0.860	0.859	0.861
Cruise OPR	-	63.4	63.5	63.7	62.5	62.8	63.0	58.4	62.0	61.9
Cruise SFC	g/kN.s	12.72	12.84	13.14	12.81	12.92	13.22	12.90	12.99	13.30
TOC SFC	g/kN.s	13.37	13.71	14.35	13.45	13.77	14.40	13.55	13.84	14.48
EOR SFC	g/kN.s	8.58	8.83	9.34	8.63	8.88	9.38	8.71	8.93	9.43
Total engine weight	kg	7252.8	6126.6	5081.2	5853.3	5095.4	4031.4	4944.9	4373.4	3431.7
Fan diameter	m	3.264	2.971	2.653	2.968	2.732	2.433	2.748	2.550	2.255
Cruise FN	kN	41.16	41.12	40.96	34.36	34.49	34.16	29.88	29.96	29.78
EOR FN	kN	200.90	199.05	194.79	167.69	166.93	162.22	145.34	145.00	141.70

Table 7: Scaling study for TF2050

APPENDIX D

Component	Parameter	Units	cruise	TOC	EOR
General	Mach no.	-	0.8	0.82	0.2
	Altitude	km	11.3	10.7	0
	dT ISA	K	0	+10	+15
	HP shaft mech. losses	kW	50	50	50
	IP shaft mech. losses	kW	50	50	50
	Total net thrust	kN	32.56	49.99	183.46
	BPR	-	16.84	16.08	16.14
	OPR	-	62.1	75.4	60.13
	Gearbox efficiency	-	0.995	0.995	0.995
	Gearbox Ratio		4.3	4.3	4.3
Fan	Fan PR	-	1.39	1.51	1.39
	Root PR	-	1.29	1.37	1.27
	Stage bypass η_{is}	-	0.95	0.92	0.93
	Stage core η_{is}	-	0.92	0.90	0.93
	Rotational speed	rpm	1705	1949	1844
IPC	IPC PR	-	2.67	2.43	2.30
	IPC η_{is}	-	0.92	0.78	0.87
	Rotational speed	rpm	7330	8380	7928
	Pressure loss IPC HPC duct	%	1.64	1.64	1.64
HPC	Pressure ratio	-	18.34	23.01	20.92
	Isentropic efficiency	-	0.87	0.85	0.86
	Exit temperature	K	860	1011	1053
	Rotational speed	rpm	13958	16439	16336
	Exit M_{ax}	-	0.272	0.272	0.272
	Exit hub/tip ratio	-	0.92	0.272	0.272
Combustor	Combustion efficiency	%	99.95	99.95	99.95
	Pressure loss	%	3	3	3
HPT	TET	K	1540	1890	1921
	HPT η_{is}	-	0.90	0.91	0.91
	$\dot{m}_{cool,rel}$	-	0.063	0.063	0.063
	T_{blade}	K	1113	1345	1380
LPT	LPT η_{is}	-	0.95	0.95	0.95
Nozzles	C_x bypass	-	0.991	0.991	0.991
	C_x core	-	0.994	0.994	0.994
	Pressure loss bypass duct	%	1.1	1.1	1.1
	Pressure loss core duct	%	1.3	1.3	1.3
Output	Thermal efficiency	-	0.53	0.54	0.46
	Propulsive efficiency	-	0.82	0.78	0.42
	Overall efficiency	-	0.44	0.42	0.20
	Specific thrust	m/s	84.6	111.3	183.1
	Engine air mass flow	kg/s	384.7	449.0	1002.2
	SFC	g/kN.s	12.60	13.73	8.28
	Total engine Weight	kg	5161.3		
	Fan diameter	m	2.840		
	Mission fuel burn	kg	$46.0 \cdot 10^3$		

Table 8: Performance of final TF2050

APPENDIX E

Component	Parameter	Units	18 kN	22.2 kN	25 kN
General	Mach no	-	0.73	0.73	0.73
	Altitude	m	10688	10688	10688
	dT ISA	K	10	10	10
	HP shaft power extraction	kW	0	0	0
	Net Thrust	N	18000	22200	25000
	OPR	-	52.78	55.82	59.22
	SFC	g/kN.s	10.85	10.61	10.35
	Core air mass flow	kg/s	8.23	10.04	11.19
CRP	Forward propeller diameter	m	4.0	4.2	4.5
	Rear propeller diameter	m	3.5	3.7	3.9
	Forward propeller loading	kW/m^2	221	221	221
	Rear propeller loading	kW/m^2	245	266	261
	Forward propeller η	-	0.83	0.83	0.83
	Rear propeller η*	-	0.82	0.82	0.82
IPC	IPC PR	-	9.46	9.72	10.02
	IPC η_{poly}	-	0.926	0.926	0.926
HPC	HPC PR	-	5.66	5.82	6.00
	HPC η_{poly}	-	0.886	0.892	0.894
	HPC LSBH	mm	10.29	11.10	11.44
Combustor	Pressure loss	%	4	4	4
	Combustion efficiency	%	99.995	99.995	99.995
HPT	Combustor outlet temperature	K	1809	1808	1808
	HPT TET	K	1750	1750	1750
	HPT η_{poly}	-	0.903	0.906	0.907
	HPT T_{blade}	K	1289	1293	1298

Table 9: Scaling study of GOR2050 (TOC thrust levels)

* The efficiency of the combined propeller is higher because the second row cancels out most of the swirl from the first row.

APPENDIX F

Component	Parameter	Units	TOC	CR	EOR
General	Mach no.	-	0.73	0.71	0.2
	Altitude	m	10688	11277	0
	dT ISA	K	10	0	15
	HP shaft power extraction	kW	0	0	0
	Net Thrust	kN	17.34	13.85	78.95
	OPR	-	41.14	36.81	33.40
	Core air mass flow	kg/s	7.08	6.17	17.43
	SFC	g/kN.s	10.75	10.41	6.44
CRP array	Forward Propeller Diameter	m	4.0	4.0	4.0
	Rear Propeller Diameter	m	3.5	3.5	3.5
	Forward Propeller loading	kW/m^2	180	136	415
	Rear Propeller loading	kW/m^2	224	170	519
	Percentage clipping	%	20	20	20
	Front propeller hub to tip ratio	-	0.38	0.38	0.38
	Forward propeller Cp	-	1.67	1.67	1.67
	Rear propeller Cp	-	1.67	1.67	1.67
	Forward propeller J	-	2.30	2.30	2.30
	Rear propeller J	-	2.30	2.30	2.30
	Forward propeller number of blades	-	15	15	15
	Rear propeller number of blades	-	13	13	13
	Forward Propeller η	-	0.83	0.87	0.58
	Rear Propeller η*	-	0.82	0.85	0.58
IPC	IPC PR	-	8.35	8.22	7.47
	IPC η_{poly}	-	0.926	0.939	0.933
	Pressure loss IPC–HPC duct	%	1.43	1.43	1.43
	Percentage bleed air	%	1.76	1.76	1.76
HPC	HPC PR	-	5.00	4.54	4.54
	HPC polytropic efficiency	-	0.890	0.892	0.891
	HPC hub/tip ratio	-	0.895	0.895	0.895
	HPC LSBH	mm	10.85	10.85	10.85
	Percentage bleed air	%	16.9	16.9	16.9
	Pressure loss HPT- burner duct	-	0.02	0.02	0.02
Combustor	Pressure loss	%	4	4	4
	Burner efficiency	%	99.995	99.995	99.995
HPT	HPT TET	K	1750	1628	1950
	HPT η_{poly}	-	0.914	0.898	0.905
	HPT T_{blade}	K	1233	1139	1374
	Pressure loss HPT-IPT duct	%	2.5	2.5	2.5
IPT	IPT entry temperature	K	1374	1269	1551
	IPT η_{poly}	-	0.951	0.946	0.945
	Pressure loss IPT-LPT duct	%	0.024	0.024	0.024
LPT	LPT entry temperature	K	1161	1072	1320
	LPT η_{is}	-	0.932	0.944	0.928
	Gas outlet temperature	K	726	672	910
	Rotational speed	rpm	9491	9491	9491
DPGB	Mechanical efficiency	-	0.988	0.985	0.994
	Torque ratio	-	1.23	1.23	1.23

Component	Parameter	Units	TOC	CR	EOR
	Heat loss	kW	43.8	41.7	54.4
	Carrier rotational speed	rpm	452	452	452
	Carrier torque	kNm	40.94	31.07	94.62
	Ring rotational speed	rpm	-452	-452	-452
	Ring torque	kNm	-37.22	-28.25	-86.02
	Sun torque	kNm	3.77	2.87	8.66
DPGB cooling system	Scoop inlet mass flow	kg/s	0.95	0.86	4.15
	Heat exchanger effectiveness	-	0.92	0.92	0.92
	Heat exchanger pressure loss	%	2	2	2
	Scoop nozzle exit area	m^2	0.013	0.013	0.013
	Scoop nozzle net thrust	N	17	16	895
Nozzle	C_x	-	0.994	0.994	0.994
	Exit area	m^2	0.243	0.243	0.243
	Nozzle pressure ratio	-	1.35	1.27	1.13
	Outlet jet velocity	m/s	287	246	210

Table 10: Performance of final GOR2050

* The efficiency of the combined propeller is higher because the second row cancels out most of the swirl from the first row

2019-10-04

Modelling geared turbofan and open rotor engine performance for year-2050 long-range and short-range aircraft

Mastropierro, Francesco Saverio

ASME

Mastropierro FS, Sebastiampillai J, Jacob F, Rolt A. (2020) Modelling geared turbofan and open rotor engine performance for year-2050 long-range and short-range aircraft. Journal of Engineering for Gas Turbines and Power. Volume 142, Issue 4, April 2020, Article number 041016, Paper number GTP-19-1447

https://doi.org/10.1115/1.4045077